Effect of internal magnetic field on collective flow in heavy ion collisions at intermediate energies

Yuliang Sun, Yongjia Wang, Qingfeng Li, and Fuqiang Wang

The effect of internal magnetic field on collective flow in heavy ion collisions at intermediate energies

Yuliang Sun [1a], Yongjia Wang [1b], Qingfeng Li [1,2c], and Fuqiang Wang [1,3d]

1) School of Science, Huzhou University,

Huzhou 313000, P.R. China

2) Institute of Modern Physics,

Chinese Academy of Sciences,

Lanzhou 730000, P.R. China

3) Department of Physics and Astronomy,

Purdue University, West Lafayette 47907, USA

(Dated: May 14, 2019)

---

[a] E-mail address: sunyl@zjhu.edu.cn

[b] E-mail address: wangyongjia@zjhu.edu.cn

[c] E-mail address: liqf@zjhu.edu.cn

[d] E-mail address: fqwang@zjhu.edu.cn

Abstract

The properties of nuclear matter under extreme conditions of high temperature, density and isospin-asymmetry have attracted wide attentions in recent years. At present, heavy ion reactions in combination with corresponding model simulations are one of the most important ways to investigate this subject. It is known that a strong magnetic field can be created in heavy ion collisions. However, its effect on the motion of charged particles is usually neglected in previous transport model simulations. In this work, within the Ultra-relativistic Quantum Molecular Dynamics (UrQMD) model, the temporal evolution and spatial distribution of the internal magnetic field are calculated. The magnetic field strength is found to reach about $eB \approx 470$ MeV^2 ($B \approx 8 \times 10^{16}$ G) for Au+Au collisions at E_{lab}=1 GeV/nucleon with impact parameter of 7 fm. The magnetic field in Cu+Au collisions exhibits somewhat different spatial distribution from that in Au+Au collisions. The magnetic field is found to affect the directed flow of pions at forward and backward rapidities to some extent, dependent of the impact parameter and beam energy while the effect on the elliptic flow is small. In addition, the effects of the magnetic field on the π^-/π^+ ratio over the whole rapidity range and the elliptic flow difference v_2^n-v_2^p between neutrons and protons at forward and backward rapidities are on the same order as those from the nuclear symmetry energy. The v_2^n-v_2^p difference in the mid-rapidity region is not strongly affected by the magnetic field, and the total π^-/π^+ yield ratio is immune to it. It is advisable to include the magnetic field effects in future studies using pion flow, pion yield ratio and nucleon elliptic flow difference to probe the symmetry energy at super saturation densities.

I. INTRODUCTION

The nuclear equation of state (EOS), a relationship involving the binding energy, nuclear matter density, isospin asymmetry and temperature, has been a continuous focus of research in nuclear physics [1–4]. In particular, the isospin degree of freedom in the nuclear EOS has attracted wide attentions in recent decades. Although the EOS of isospin symmetric nuclear matter is relatively well constrained to a narrow region (its incompressibility K_0 is in the range of 200-260 MeV) [5–8], the EOS of isospin asymmetric nuclear matter is still poorly understood [9–12]. The largest uncertainty comes from the density dependence of the nuclear symmetry energy. Knowledge of the nuclear symmetry energy is important for understanding the properties of exotic nuclei, heavy-ion reactions with radioactive beams, and the structure of neutron stars [3, 4, 13–16]. Heavy-ion collision experiments combined with model simulations are among the most important ways to investigate the EOS and the nuclear symmetry energy at high densities. A number of theoretical and experimental studies of the nuclear symmetry energy have been carried out. Until very recently, the nuclear symmetry energy at subnormal densities is relatively well constrained, but its high-density behavior is still poorly known [9, 10, 17–24].

It was first pointed out by Rafelski and Müller [25] that, in addition to strong electric field, strong magnetic field is also created in heavy-ion collisions (HICs). In sub-Coulomb barrier U+U collisions, the magnetic field was estimated to be on the order of 10^{14} G [25]. More recently, it was shown by Kharzeev et al. [26] that HICs at the Relativistic Heavy Ion Collider (RHIC) and the Large Hadron Collider (LHC) can create the strongest magnetic field ever achieved in a terrestrial laboratory. For example, in noncentral Au + Au collisions at 100 GeV/nucleon, the maximal magnetic field can reach about 10^{18} G [26].

The strong magnetic field generated by heavy ion collisions in the relativistic energy region has recently attracted intense attention [26–28], but its effect in the intermediate to low energy regions has not been thoroughly investigated. Ou and Li [29] studied the temporal evolution and spatial distribution of internal electromagnetic fields in heavy-ion reactions within an isospin-dependent Boltzmann-Uhling-Uhlenbeck(IBUU) transport model, and found that the inner magnetic field had almost no effect on nucleon observables, but affected the pions at large rapidities. On the other hand, the two different frameworks of IBUU and Ultra-relativistic Quantum Molecular Dynamics (UrQMD) models have been

simulated and compared in terms of sensitive probes of nuclear symmetry energy [30, 31]. It was found that the neutron to proton ratio, the π^-/π^+ ratio, and the isospin-sensitive transverse and elliptic flows from the two transport models are not always the same [30, 31]. This motivated us to investigate the effects of the inner magnetic field in the UrQMD model. We study both the symmetric Au+Au and asymmetric Cu+Au collisions because the magnetic fields are expected to differ between these two systems. It is expected that anisotropic flow would be affected by the magnetic field, so we investigate the effects of the magnetic fields on directed flow and elliptic flow in Au+Au and Cu+Au collisions. This is particularly relevant for directed flow which has been extensively studied in Au+Au and Cu+Au at low energies [32, 33].

The rest of the paper is organized as follows. In the next section, we describe the UrQMD model and how the calculation of the internal magnetic field is implemented in the UrQMD model. The characteristics of the magnetic field and its effects on the collective flow, observables in heavy-ion collisions at intermediate energies are discussed in Sec. III, IV and V, respectively. Sec. VI summarizes our work.

II. MAGNETIC FIELD CALCULATIONS IN URQMD

The UrQMD model [34–37] has been widely and successfully used in the studies of pp, pA, and AA collisions over a large range of energy from Bevalac and SIS up to the AGS, SPS, RHIC, and LHC. At lower energies, the UrQMD model is based on principles analogous to the quantum molecular dynamics (QMD) model [38] in which each nucleon is represented by a Gaussian wave packet in phase space. The centroids $\mathbf{r}_i$ and $\mathbf{p}_i$ of a hadron i in the coordinate and momentum spaces are propagated according to Hamilton's equations of motion:

$$\dot{\mathbf{r}}_i = \frac{\partial H}{\partial \mathbf{p}_i}, \qquad \text{and} \qquad \dot{\mathbf{p}}_i = -\frac{\partial H}{\partial \mathbf{r}_i}. \tag{1}$$

The total Hamiltonian H consists of the kinetic energy T and the effective two-body interaction potential energy U,

$$H = T + U. \tag{2}$$

In this work, the mean field potential part is derived from the Skyrme energy density functional, and the SV-mas08 [6] interaction with a corresponding incompressibility K_0=233
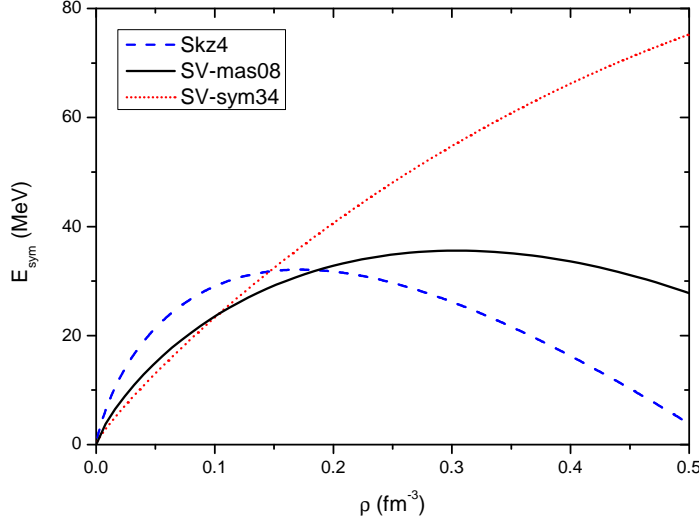
4

FIG. 1. (Color online) The nuclear symmetry energy obtained from Skz4, SV-mas08 (default), and SV-sym34 are shown as a function of density.

MeV is employed throughout the paper without explicit mention. In order to assess the impact of the magnetic filed on the extraction of the nuclear symmetry energy from isospin sensitive observables, two more interactions (Skz4 and SV-sym34) which give different values of the slope parameter of the nuclear symmetry energy are introduced. The nuclear symmetry energy obtained from those three interactions are displayed in Fig. 1. The implementation of medium modifications for nucleon-nucleon elastic cross sections and Pauli blocking is consistent with Ref. [39]. The experimental data of heavy-ion collisions in intermediate energies can be reproduced reasonably well by this model [39–45].

The coulomb field has already been considered in most transport models. The magnetic field at field point $\mathbf{r}_i$ (the ith particle's position) produced by particle motions can be calculated by the Liénard-Wiechert potentials as in Ref. [46]:

$$e\mathbf{B}(\mathbf{r}_i, t) = \frac{e^2}{4\pi\varepsilon_0 c} \sum_j Z_j \frac{c^2 - |\mathbf{v}_j|^2}{(c|\mathbf{R}_j| - \mathbf{R}_j \cdot \mathbf{v}_j)^3} \mathbf{v}_j \times \mathbf{R}_j \bigg|_{\text{Retarded}}. \tag{3}$$

Here Z_j is the charge number of the jth particle; $\mathbf{R}_j = \mathbf{r}_i - \mathbf{r}_j$ is the field point $\mathbf{r}_i$ relative to the position $\mathbf{r}_j$ of the particle j moving at velocity $\mathbf{v}_j$, taken at retarded time [46]. For constant $\mathbf{v}_j$ (e.g. of spectator protons), Eq. (3) reduces to [46]

$$e\mathbf{B}(\mathbf{r}_i, t) = \frac{e^2}{4\pi\varepsilon_0 c} \sum_j Z_j \frac{c^2 - |\mathbf{v}_j|^2}{((c|\mathbf{R}_j|)^2 - (\mathbf{R}_j \times \mathbf{v}_j)^2)^{3/2}} \mathbf{v}_j \times \mathbf{R}_j, \tag{4}$$

5

where $\mathbf{r}_j$ and $\mathbf{v}_j$ are now taken at the time instant t.

For participant charged particles, the retardation effect is tedious to implement because of the changes of their velocities. One approach is to use the non-relativistic approximation by assuming $\mathbf{v}_j/c \ll 1$ in Eq. (3), namely

$$e\mathbf{B}(\mathbf{r}_i, t) = \frac{e^2}{4\pi\varepsilon_0 c^2} \sum_j Z_j \frac{1}{|\mathbf{R}_j|^3} \mathbf{v}_j \times \mathbf{R}_j. \tag{5}$$

In order to see how large the effect of relativity is, we compare the values of $-eB_y(0, 0, 0)$ produced by spectators protons in Au+Au collisions at the beam energy E_{lab}=1 GeV/nucleon calculated by Eq. (4) and by the non-relativistic approximation of Eq. (5). These are shown as the red dash curves and blue dash dot curves in Fig. 2, respectively. The $-eB_y$ is plotted in unit of MeV^2, which is equal to 1.7×10^{14} G. The effect of relativity is approximately $+20\%$ at time $t \lesssim 20$ fm/c. At later times, the effect reverses sign. The relative effect is larger, but since the magnetic field is relatively small, the effect is not expected to affect our results significantly. Note, in UrQMD, $t = 0$ is always defined to be the time instant when the surface distance between the two nuclei is 1.6 fm.

Since particles are treated as point-like, singularities appear when $\mathbf{R}_j = 0$. In order to avoid the singularity by effectively considering the size of the particles, the magnetic field produced by particle j is ignored in the above calculation when $|\mathbf{R}_j| < 1$ fm (using smaller cutoff values yielded consistent results). To avoid the singularity problem all together, and arguably more physically motivated, one many use Gaussian wave packets instead of point-like particles. To consider wave packet in calculating the magnetic field by particle j at field point $\mathbf{r}_i$, we first obtain the vector potential [47]:

$$\mathbf{A}_j(\mathbf{r}_i, t) = \frac{e}{4\pi\varepsilon_0 c^2} \mathbf{v}_j \int \rho_i(\mathbf{r}, t) \frac{1}{\mathbf{r} - \mathbf{r}'} \rho_j(\mathbf{r}', t) d\mathbf{r} d\mathbf{r}'. \tag{6}$$

Here

$$\rho_i(\mathbf{r}, t) = \frac{1}{(2\pi\sigma_r^2)^{3/2}} \exp\left(-\frac{(\mathbf{r} - \mathbf{r}_i(t))^2}{2\sigma_r^2}\right), \tag{7}$$

with $\sigma_r^2 = 2$ fm^2 being the width parameter of Gaussian. The magnetic field is then given by

$$\mathbf{B}_j(\mathbf{r}_i, t) = \triangledown \times \mathbf{A}_j(\mathbf{r}_i, t), \tag{8}$$

and the total magnetic field

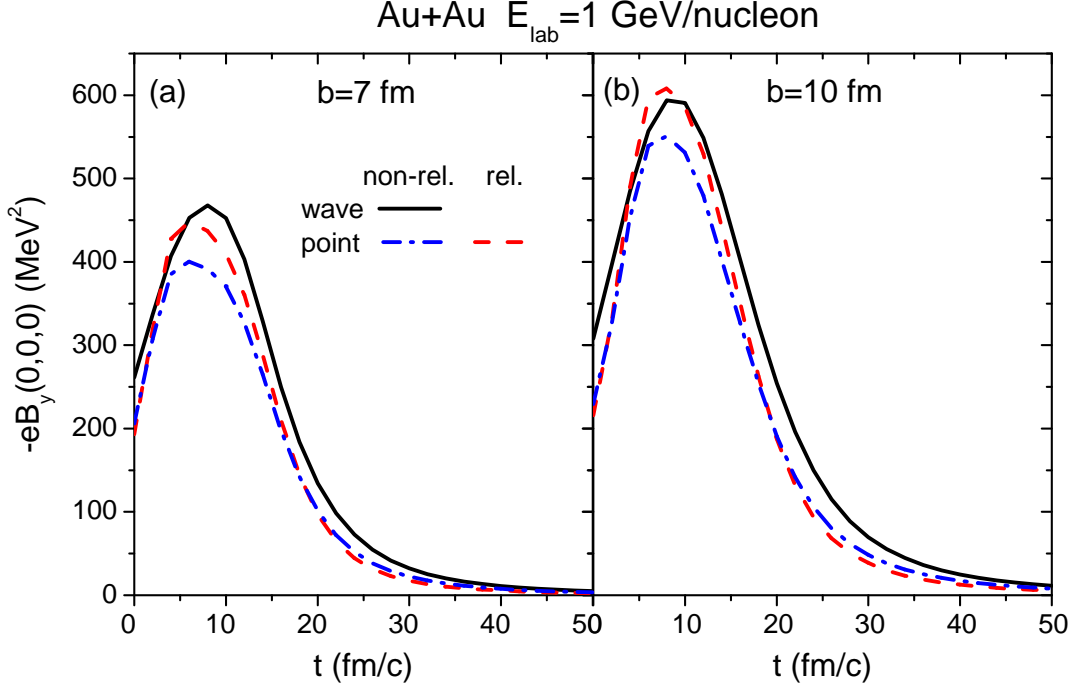$$\mathbf{B}(\mathbf{r}_i, t) = \sum_j \mathbf{B}_j(\mathbf{r}_i, t)$$

FIG. 2. (Color online) Temporal evolution of the magnetic field component $-eB_y(0,0,0)$ produced by spectator protons in Au+Au collisions at the beam energy E_{lab}=1 GeV/nucleon with (a) $b=7$ fm and (b) $b=10$ fm. The legend "non-rel. wave", "non-rel. point" and "rel. point" indicate the results obtained using Eqs. (10), (5) and (4), respectively.

produced by all particles can be obtained. Because UrQMD has already computed the electric potential in its coding implementation,

$$e\Phi_j(\mathbf{r}_i, t) = \frac{e^2}{4\pi\varepsilon_0} \times \int \rho_i(\mathbf{r}, t)\frac{1}{\mathbf{r} - \mathbf{r}'}\rho_j(\mathbf{r}', t)d\mathbf{r}d\mathbf{r}', \tag{9}$$

the magnetic field strength can be readily calculated by

$$e\mathbf{B}_j(\mathbf{r}_i, t) = \triangledown \times e\mathbf{A}_j(\mathbf{r}_i, t) = \triangledown \times (\frac{e}{c^2}\Phi_j(\mathbf{r}_i, t)\mathbf{v}_j) = -\frac{e}{c^2}\mathbf{v}_j \times \triangledown\Phi_j(\mathbf{r}_i, t). \tag{10}$$

We note here that the relativistic effect is not considered in this method. $-eB_y(0,0,0)$ produced by spectators protons in Au+Au collisions at the beam energy E_{lab}=1 GeV/nucleon calculated by Eq. (10) are shown as the black solid curves in Fig. 2.

In principle, the magnetic field strength should be calculated by the relativistic formula of Eq. (3). However, it is hard to implement for participant charged particles because their velocities change over time. We thus examine next the relative contributions to the

magnetic field from participants and spectators using the non-relativistic approx imation of Eq. (10). Figure 3 is the magnetic field strengths $-eB_y(0,0,0)$ produced by participants and spectators, respectively, in Au+Au collisions at the beam energy E_{lab}=1 GeV/nucleon. The magnetic field strengths produced by participants and spectators are both dependent of the impact parameter (b) because the numbers of participants and spectators vary with b. The magnetic field strength produced by participants is considerable, especially in central collision, and thus can not be neglected. We therefore opt for the non-relativistic wave-packet calculations Eq. (10) in this work, with the understanding that the relativistic correction is on the order of $+20\%$ at $t \lesssim 15$ fm/c when the magnetic field is appreciable. Since, as we will show, the influence of magnetic field on our observables is generally small, less than 10%, the approximation on the magnetic field introduces an uncertainty on the results of this work only by a few percent, without changing the qualitative conclusions.
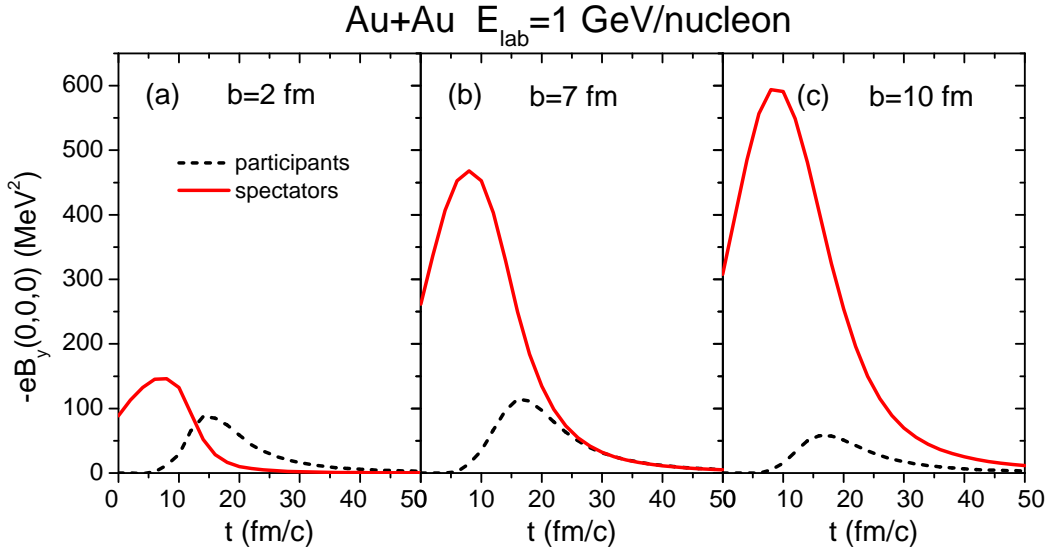

FIG. 3. (Color online) The magnetic field strengths $-eB_y(0,0,0)$ produced by participants or spectators in Au+Au collisions at the beam energy E_{lab}=1 GeV/nucleon with impact parameter b=2, 7, 10 fm.

The Lorentz force on the charged particle i can be written as

$$\mathbf{F}_{i(mag)} = Z_i \mathbf{v}_i \times e\mathbf{B}(\mathbf{r}_i, t). \tag{11}$$

To take into account the effect of inner magnetic field in the UrQMD model, in the quasi-

particle approximation, the Lorentz force is added to Eq. (12), namely

$$\dot{\mathbf{r}}_i = \frac{\partial H}{\partial \mathbf{p}_i}, \qquad \text{and} \qquad \dot{\mathbf{p}}_i = -\frac{\partial H}{\partial \mathbf{r}_i} + \mathbf{F}_{i(mag)}. \qquad (12)$$

We note that the URQMD calculation here is carried out with mean field potential, and the evolution of the collision system including all particles is computed until the last step of the model simulation. This includes the computations of the magnetic field influence on particles' motion.

III.   MAGNETIC FIELD RESULTS IN HEAVY-ION COLLISIONS

We take the z-axis as the beam direction and x-axis as the impact parameter direction. In the limit of smooth nuclear density, because of symmetry, only the y component of the magnetic field is non-vanishing. On event-by-event basis, because of fluctuations, all x, y, z components of the magnetic field are present [27]. In our simulation, all three components of the magnetic field are calculated and included in the Lorentz force of Eq. (11). Averaged over many events, the x, z components of the magnetic field vanish, and only the y component remains. For the flow variables we study which are event-averaged quantities, only the B_y component will have an effect. In this section we depict the y component of the magnetic field averaged over many events.

Figure 4 shows the magnetic field strength $-eB_y$ in the $y = 0$ plane at $t = 0, 10, 20, 30$ fm/c in Au+Au (top) and Cu+Au (bottom) collisions at the beam energy E_{lab}=1 GeV/nucleon with impact parameter $b = 7$ fm. In the overlap zone ($|x| \lesssim 5$ fm), the magnetic fields generated by the two spectators add up as they are both in the $-y$ direction. The strength of the magnetic field peaks when the two nuclei reach the maximum compression and drops when the nuclei depart from each other. The magnetic fields in the outer regions ($|x| \gtrsim 5$ fm) partially cancel each other as the magnetic fields from the two spectators are in the opposite directions in y. In Cu+Au collisions, the magnetic field generated by the Cu nucleus is smaller than that by the Au nucleus at the same distances of the field point, so the two magnetic fields largely cancel each other in the $+x$ direction but only partially at $-x$ direction. The largest magnitude magnetic field is not at the origin.

The magnetic field $-eB_y(x, 0, 0)$ is shown as a function of time for various transverse coordinate x in Fig. 5(a) Au+Au and (b) Cu+Au. The magnetic field strength increases
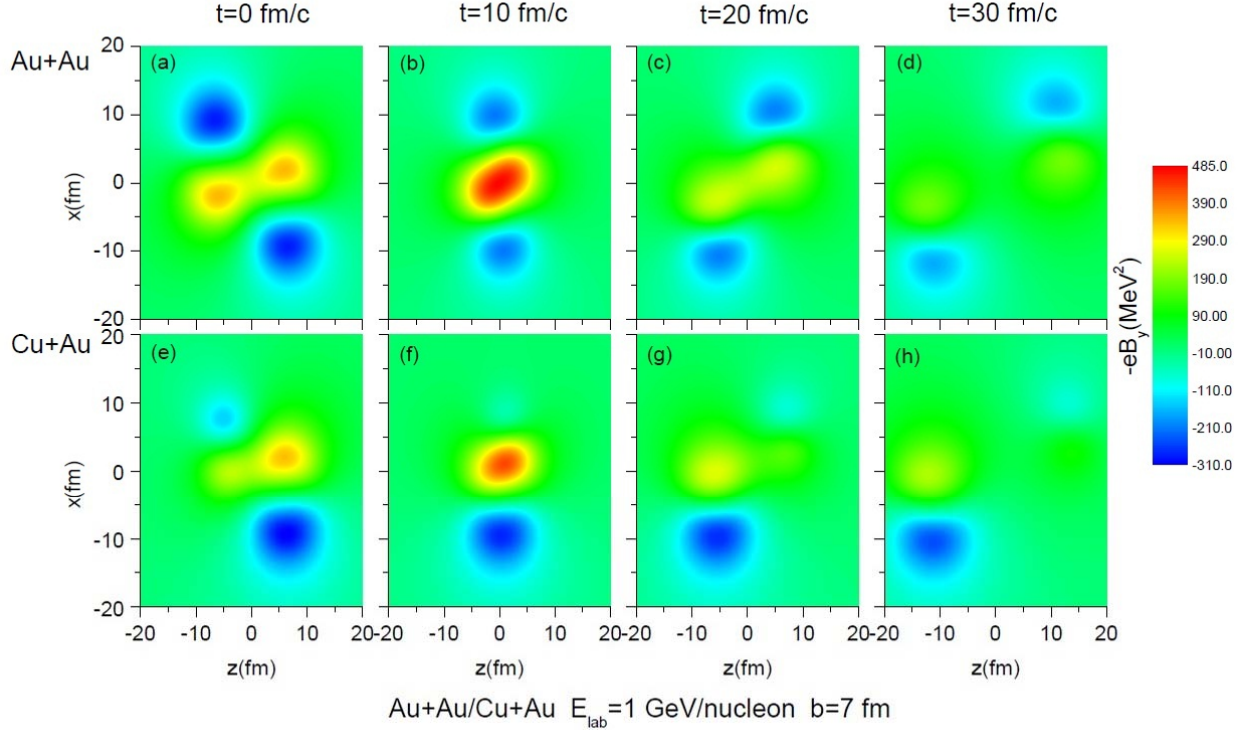
FIG. 4. (Color online) Distributions of the magnetic field strength $-eB_y$ in the reaction plane at $t = 0, 10, 20, 30$ fm/c in Au+Au (top) and Cu+Au (bottom) collisions at the beam energy E_{lab}=1 GeV/nucleon with impact parameter $b = 7$ fm.

with time, reaches about $eB \approx 470$ MeV^2 ($B \approx 8 \times 10^{16}$ G) at $t = 10$ fm/c, and then decreases with increasing time. The magnetic field is strongest in the central region and decreases with increasing x. There are several differences in Cu+Au compared to Au+Au: the largest magnetic field strength is at $x \approx 1$ fm instead of $x = 0$; the peaks of the magnetic field strength appear later in the $x > 0$ region (Cu side) and earlier in the $x < 0$ region (Au side); and the magnetic field strengths at some places of $x > 0$ in Cu+Au are stronger than those in Au+Au, although the magnetic field strength in the center is weaker than that in Au+Au. The magnetic field $-eB_y(0, y, 0)$ as a function of time for various y positions is present in Fig. 5(c) Au+Au and (d) Cu+Au. The magnetic field strength decreases with increasing y, the distance from the reaction plane.

Shown in Fig. 6 is the maximum of $-eB_y(0, 0, 0)$ as functions of the impact parameter b in Au+Au/Cu+Au collisions at the beam energy E_{lab}=1 GeV/nucleon. The strength of the magnetic field increases with increasing impact parameter b, and then decreases with increasing b. The dependence is understood because of the interplay of the number of
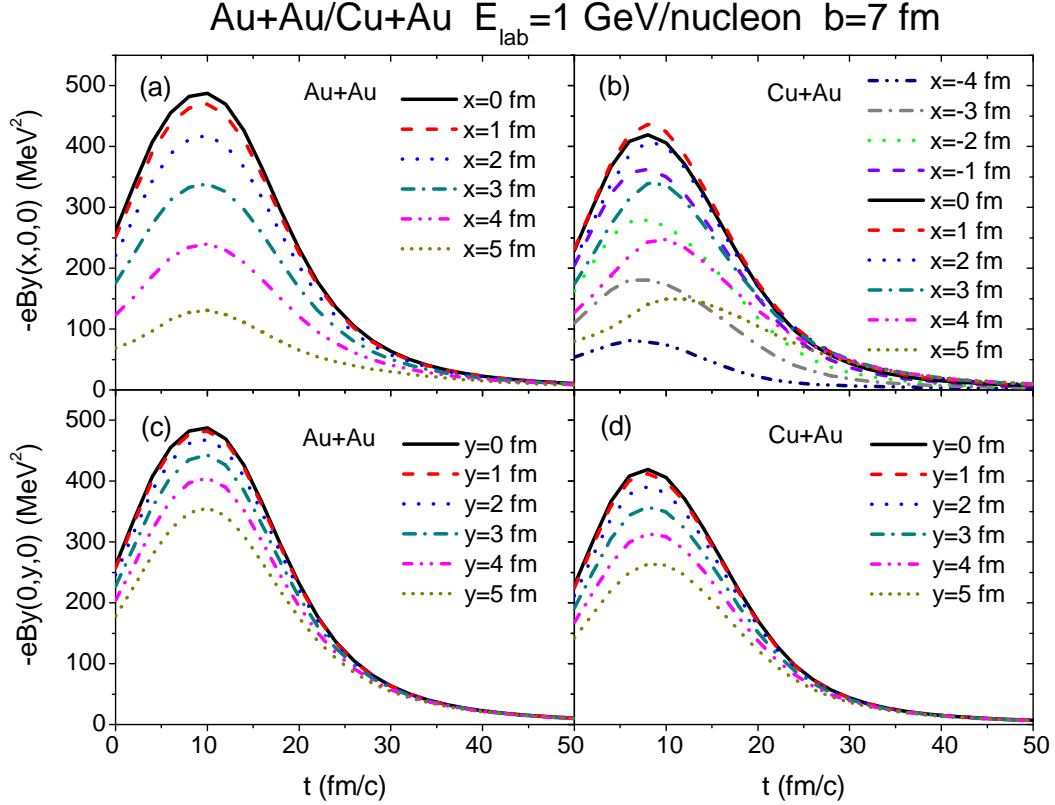
10

FIG. 5. (Color online) Temporal evolution of the magnetic field $-eB_y$ at the point $(x, 0, 0)$ in (a) Au+Au and (b) Cu+Au, and at the point $(0, y, 0)$ in (c) Au+Au and (d) Cu+Au at the beam energy E_{lab}=1 GeV/nucleon with impact parameter $b = 7$ fm.

spectator protons and the distances of the center $(0,0,0)$ from those spectator protons.

Figure 7 is the beam energy dependence of $-eB_y(0, 0, 0)$ in Au+Au/Cu+Au collisions with $b = 7$ fm. The magnetic field reaches maximum at shorter times at higher energies as expected. The magnetic field increases with increasing beam energy, while the duration of the magnetic field decreases because the spectators leave the collision region more quickly at higher beam energies. Both the magnetic field strength and duration are important for observable effects. We thus show in Fig. 8 the more relevant integral quantity,

$$\int_0^\infty -eB_y(0,0,0)dt \approx \int_0^{100\text{fm/c}} -eB_y(0,0,0)dt,$$

as a function of beam energy in Au+Au/Cu+Au collisions with $b = 7$ fm. Only weak energy dependence is observed for this quantity.

11
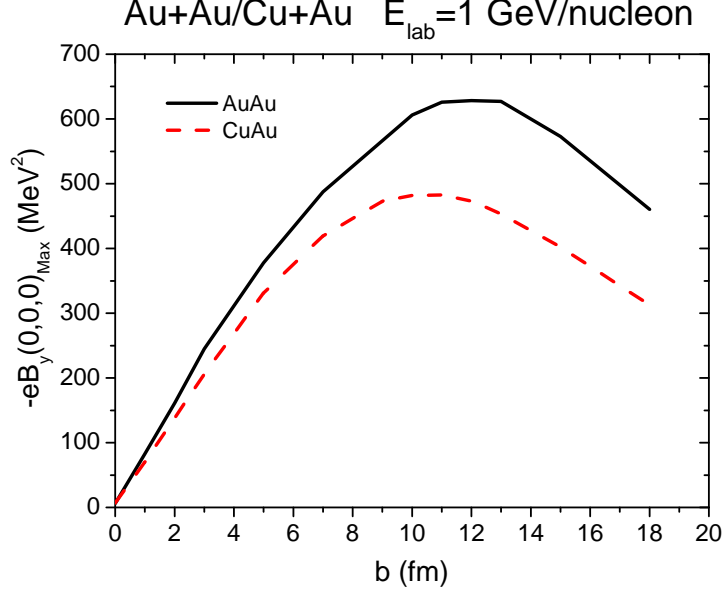
Au+Au/Cu+Au E_{lab}=1 GeV/nucleon

FIG. 6. (Color online) The peak value of the time evolution of $-eB_y(0,0,0)$ as a function of the impact parameter b in Au+Au/Cu+Au collisions at the beam energy E_{lab}=1 GeV/nucleon.
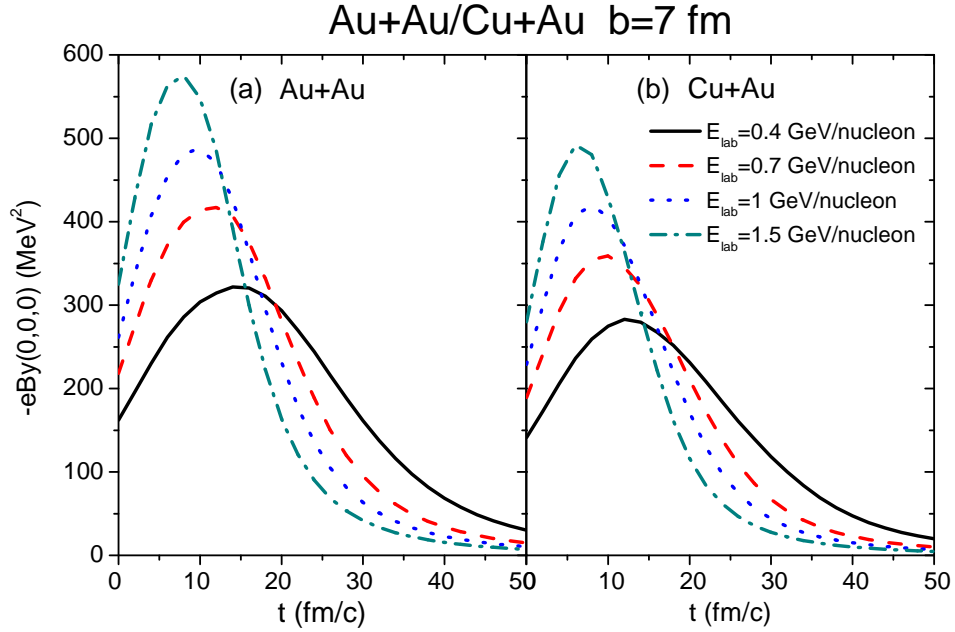
Au+Au/Cu+Au b=7 fm

FIG. 7. (Color online) Beam energy dependence of $-eB_y(0, 0, 0)$ in (a) Au+Au and (b) Cu+Au collisions with $b = 7$ fm.
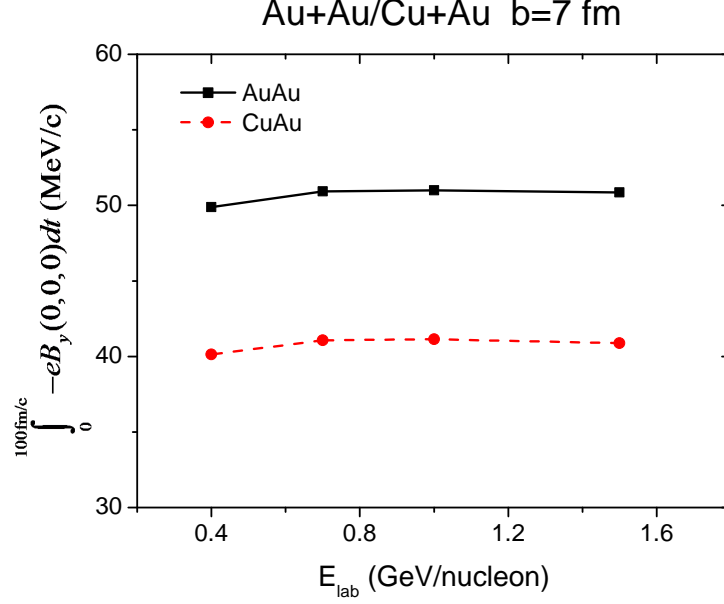
12

FIG. 8. (Color online) The integral of $\int_0^\infty -eB_y(0,0,0)dt \approx \int_0^{100\text{fm/c}} -eB_y(0,0,0)dt$ as a function of beam energy in Au+Au and Cu+Au collisions with $b = 7$ fm.

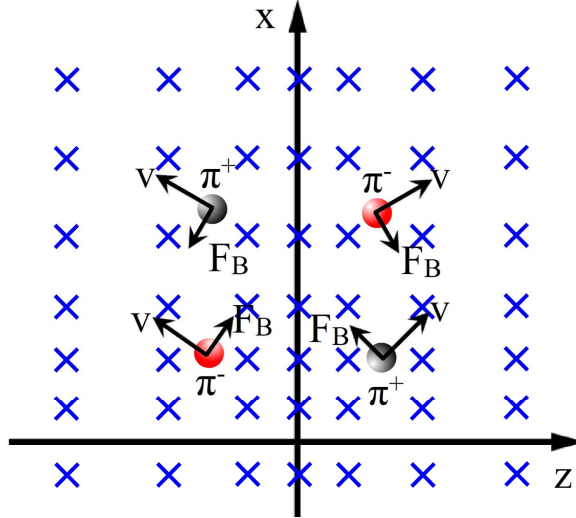## IV.   MAGNETIC EFFECTS ON THE COLLECTIVE FLOW OF PIONS

FIG. 9. (Color online) A sketch illustrating the Lorentz force on charged pions.

From the expression of the Lorentz force of Eq. (11), it is easy to see that the main component of the Lorentz force is in the x direction because the average magnetic filed is in the y direction. The x component of the average momentum, $\langle p_x \rangle$, is thus a quantity

13

most likely to be affected. This is illustrated in Fig. 9. The Lorentz force deflects the π^+ direction of motion; p_x increase (decrease) if $p_z > 0$ ($p_z < 0$). The effect on π^- is opposite. Figure 10 (a) shows the change in $\langle p_x \rangle$ due to the magnetic field for protons and pions as a function of the center-of-mass rapidity $y = \frac{1}{2}\ln(E + p_z)/(E - p_z)$ in Au+Au collision at E_{lab}=1 GeV/nucleon with $b = 7$ fm. We use the scaled units $y_0 \equiv y/y_{pro}$ as done in [48], and the subscript *pro* denotes the incident projectile in the center-of-mass system. The larger the rapidity (hence and average p_z), the larger the change in $\langle p_x \rangle$ as expected from the Lorentz force. The changes in forward and backward rapidities are on the order of 5 MeV/c. This is smaller than shown in Fig. 8 because there the time integral is for the maximum magnetic field at the center of the collision zone. The change for $\pi^\pm$ are opposite in sign because of the opposite charges. The changes for proton and π^+ are similar because the z component of the velocity, $\frac{p_z}{E} = \tanh y$, is independent of particle species. Note that even though the x and z component of the magnetic field, due to fluctuations, do not vanish from point to point on an event-by-event basis, the averages of their effects diminish. This is shown by the zero change in $\langle p_y \rangle$, as example, in Fig. 10 (b). Fig. 11 shows the $\langle p_x \rangle$ of (a) protons and (b) pions as a function of rapidity in Au+Au collision at E_{lab}=1 GeV/nucleon with $b = 7$ fm. The change in the pion p_x is obvious. The change in proton $\langle p_x \rangle$ is not noticeable because the proton $\langle p_x \rangle$ is 20 times than pion (note the different coordinate scales in Fig. 11). The proton $\langle p_x \rangle$ is large because of its large mass and the large nuclear force they experience, much larger than the magnetic Lorentz force. In present model, the motion pions only affected through pion-hadron collisions and the Coulomb field. Therefore, the effect of magnetic field on the pion flow is more obvious than that on the flow of proton.

Since the $\langle p_x \rangle$ is affected by the magnetic field, we examine the influence of the inner magnetic field on the directed flow ($v_1 = \langle \frac{p_x}{\sqrt{p_x^2 + p_y^2}} \rangle$) and the elliptic flow ($v_2 = \langle \frac{p_x^2 - p_y^2}{p_x^2 + p_y^2} \rangle$). Figure 12 shows v_1 and v_2 of protons as functions of normalized center-of-mass rapidity in Au+Au collisions at E_{lab}=1 GeV/nucleon with impact parameters of 1, 3, 5, 7 fm. No much magnetic effect is observed on protons which is consistent with Fig. 11 (a).

Figure 13, 14 show v_1 and v_2 of charged pions as a function of normalized center-of-mass rapidity in Au+Au and Cu+Au collisions at E_{lab}=1 GeV/nucleon with impact parameters of 1, 3, 5, 7 fm. Significant effects of the magnetic field are observed on the pion directed flow. The effects are larger at more forward and backward rapidities because of the larger velocity and hence larger Lorentz force. The effects increase with increasing impact parameter from
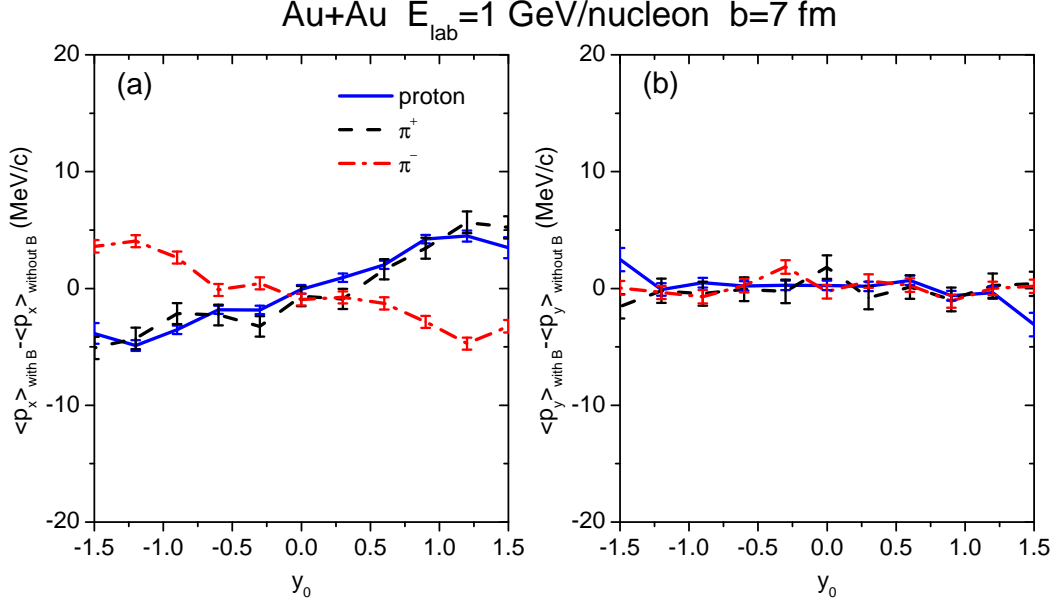
14

Au+Au E$_{\text{lab}}$=1 GeV/nucleon b=7 fm

FIG. 10. (Color online) The change of protons and pions' (a) $\langle p_x \rangle$ and (b) $\langle p_y \rangle$ by the Lorentz force as a function of normalized center-of-mass rapidity in Au+Au collision at E_{lab}=1 GeV/nucleon with $b = 7$ fm.

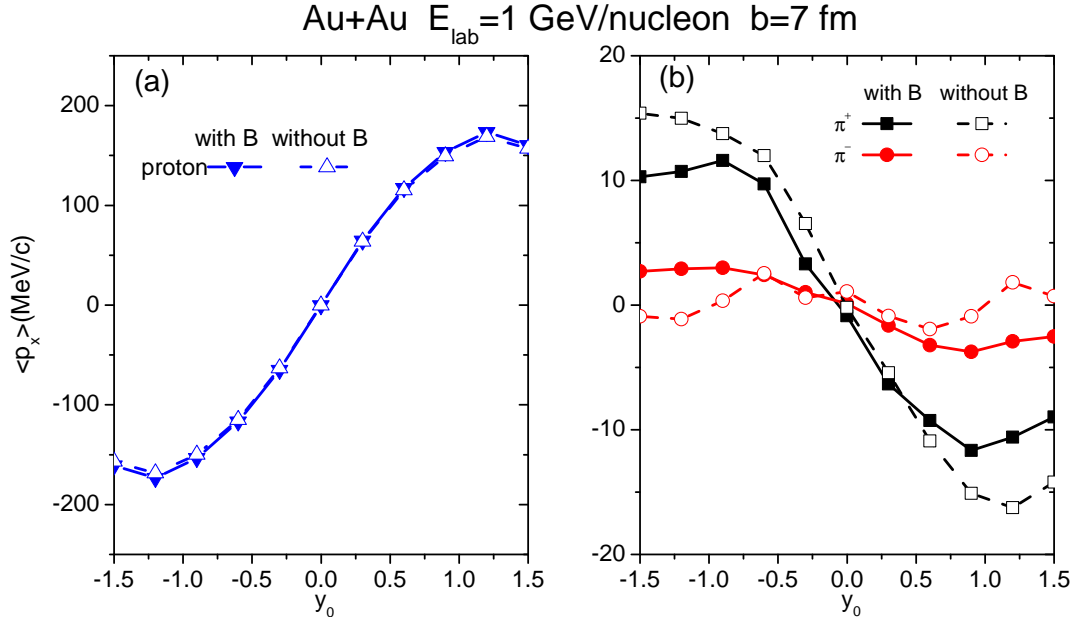Au+Au E$_{\text{lab}}$=1 GeV/nucleon b=7 fm

FIG. 11. (Color online) $\langle p_x \rangle$ of (a) protons and (b) pions as a function of normalized center-of-mass rapidity in Au+Au collision at E_{lab}=1 GeV/nucleon with $b = 7$ fm.
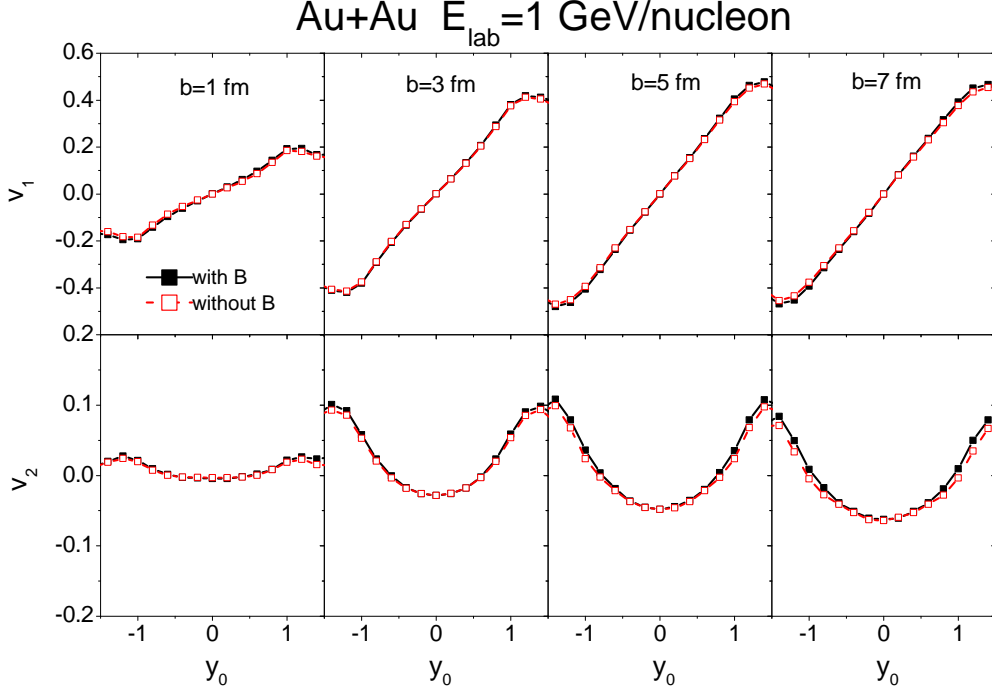
FIG. 12. (Color online) v_1 and v_2 of protons as a function of normalized center-of-mass rapidity in Au+Au collisions at E_{lab}=1 GeV/nucleon with impact parameters of 1, 3, 5, 7 fm.

1 fm to 7 fm due to the increase of the magnetic field strength. The results are consistent with Fig. 11 (b): The inner magnetic field changes the $\langle p_x \rangle$ of pions at large forward and backward rapidities. So v_1 of pions change accordingly. As seen from Fig. 11 (b), the effect of the magnetic field reduces the absolute values of $\langle p_x \rangle$ for both π^+ and π^-. Thus the v_2 of $\pi^{\pm}$ decreases at both forward and backward rapidities. This seems much more evident in Fig. 13, especially for $b = 7$ fm.

Figures 15 and 16 are v_1 and v_2 of charged pions as a function of normalized center-of-mass rapidity in Au+Au and Cu+Au collisions at E_{lab}=0.6, 1, 1.5 GeV/nucleon with b=7 fm. The effects of the magnetic field have a weak energy dependence. This is because of the interplay between the magnitude and the duration of the magnetic field, as shown in Figs. 7 and 8.

Our results of the magnetic field effect on particle anisotropic flows are qualitatively consistent with the IBUU model results of Ref. [29] in that the flows change in the same direction. However, our UrQMD results are quantitatively different from those of IBUU because of the different physical ingredients in these two models, such as the equations of state
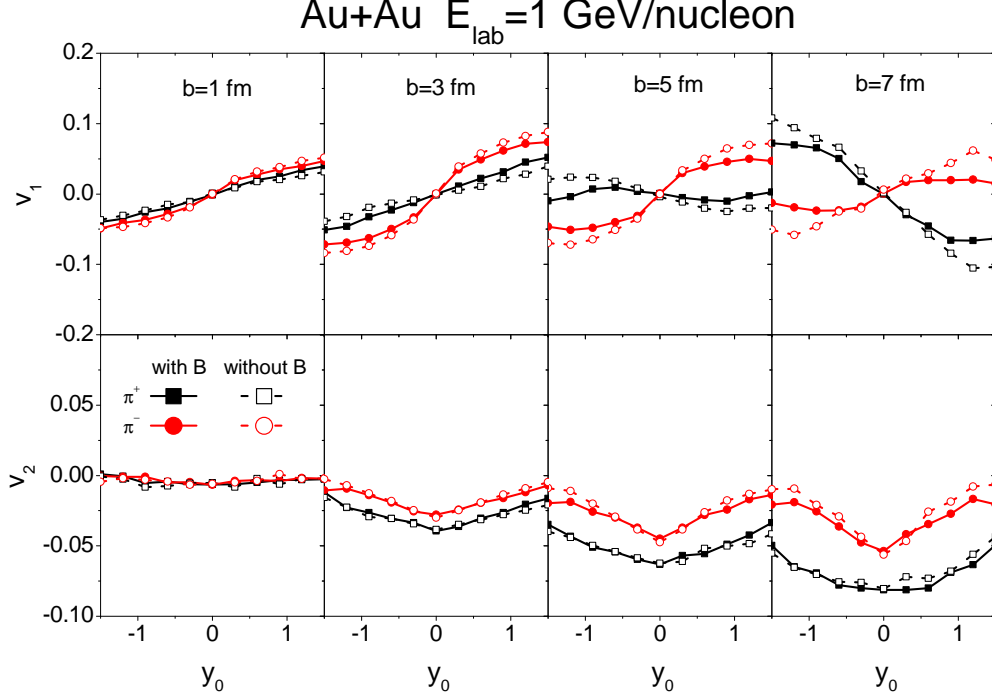
16

FIG. 13. (Color online) v_1 and v_2 of charged pions as a function of normalized center-of-mass rapidity in Au+Au collisions at E_{lab}=1 GeV/nucleon with impact parameters of 1, 3, 5, 7 fm.

and the two-bodies interaction cross sections. Nevertheless, It is clear from the calculations of both models that the pion directed flow is significantly affected by the magnetic field.

V. MAGNETIC EFFECTS ON ISOSPIN SENSITIVE OBSERVABLES

It is well known that the π^-/π^+ yield ratio and the elliptic flow difference v_2^n-v_2^p between neutrons and protons produced in HICs at intermediate energies are sensitive probes to the nuclear symmetry energy at high densities [17–19, 39, 49]. We have shown in section IV that the motion of pions and protons are influenced by the magnetic field, thus it is interesting to examine the effect of magnetic field on the π^-/π^+ and v_2^n-v_2^p with different symmetry energy parameterizations. To this end, we repeat our simulations with the Skz4 and SV-sym34 symmetry energy shown in Fig. 1. The results obtained from the default one (SV-mas08) lie in between those from Skz4 and SV-sym34.

Fig. 17 shows the π^-/π^+ as a function of rapidity calculated with different mean field potentials and with or without magnetic field. First, at both E_{lab}=0.4 and 1 GeV/nucleon,
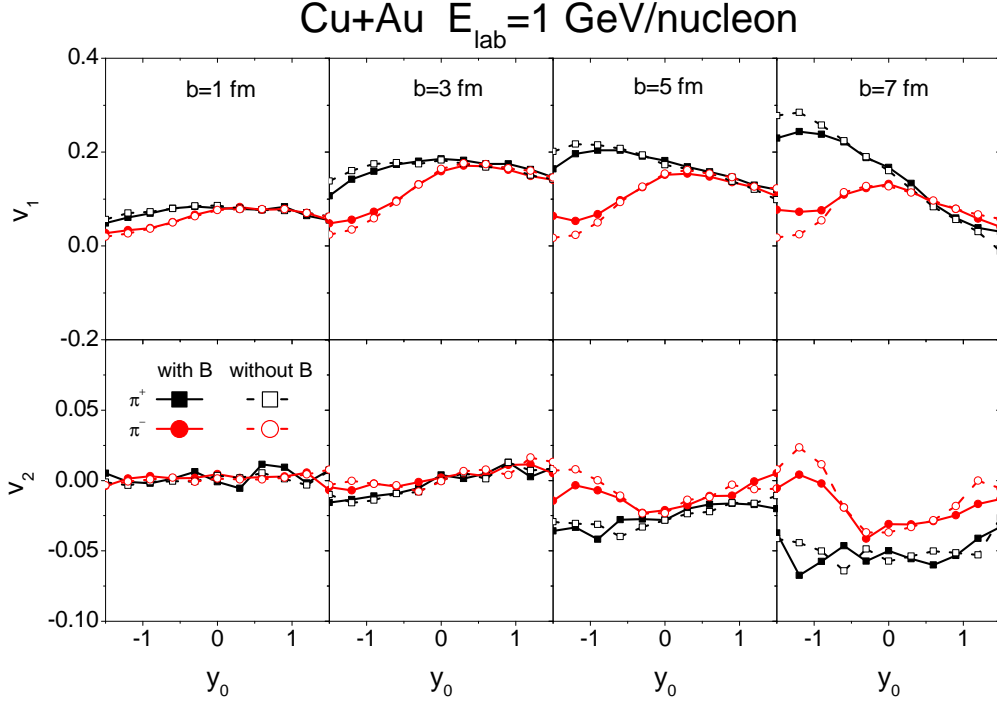
FIG. 14. (Color online) v_1 and v_2 of charged pions as a function of normalized center-of-mass rapidity in Cu+Au collisions at E_{lab}=1 GeV/nucleon with impact parameters of 1, 3, 5, 7 fm.

the magnetic field enhances the π^-/π^+ ratio at mid-rapidity region but depresses it at forward and backward rapidities, due to the magnetic focusing and defocusing effects on the positive and negative pions [29]. We have checked that the total π^-/π^+ yield ratio remains the same for calculations with and without magnetic field, as it should and also consistent with the results reported in Ref. [29]. Second, one sees clearly that the π^-/π^+ ratio in the mid-rapidity region obtained with Skz4 and without magnetic field is rather close to the result obtained with SV-sym34 and with magnetic field, illustrating that the effect of magnetic field on this observable is on the same order as the nuclear symmetry energy. This result is different from the result of Ref. [29], in which the symmetry energy effect on π^-/π^+ ratio is larger than the magnetic field effect. This difference may stem from the different treatments of pion production in the models. We note that many other physical effects (e.g., in-medium cross sections, pion dispersion relation, Δ production and decay) can significantly affect the sensitivity of π^-/π^+ ratio on the density-dependent symmetry energy [50–55], which deserve further studies.

Fig. 18 shows the v_2^n-v_2^p as a function of rapidity calculated with different mean field po-
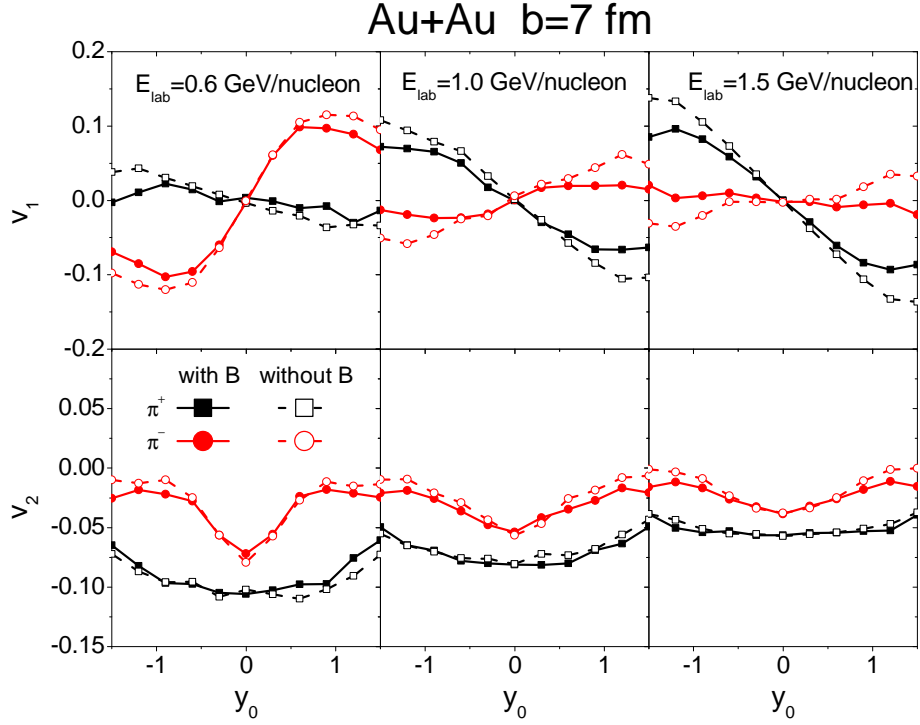
FIG. 15. (Color online) v_1 and v_2 of charged pions as a function of normalized center-of-mass rapidity in Au+Au collisions at E_{lab}=0.6, 1, 1.5 GeV/nucleon with b=7 fm.

tentials and with or without magnetic field. The effect of magnetic field is smaller than that of symmetry energy in the mid-rapidity region, especially at 0.4 GeV/nucleon, where one expects the effect of symmetry energy to be more evident. While at forward and backward rapidities, the effect of the magnetic field is on the same order as the nuclear symmetry energy. There, the v_2^n-v_2^p calculated with magnetic field is smaller than that without, because the magnetic field enhances the in-plane emission of positive charged particles, as observed in Fig. 12. These effects make the v_2^n-v_2^p dependence on rapidity more shaped with magnetic field than without, which could be taken as an indicator for the presence of the magnetic field. In addition, the magnetic effects on the transverse-momentum-dependent flow difference v_2^n-v_2^p are displayed in Fig. 19. The results from E_{lab}=0.4 and 1.0 GeV/nucleon within two rapidity windows are presented. Calculations with and without magnetic field track each other closely, illustrating the weak effect of magnetic field on the transverse-momentum dependence of the nucleon elliptic flow difference. This is presumably because high-u_{t0} particles are emitted early and escape the interaction zone quickly in the collision,
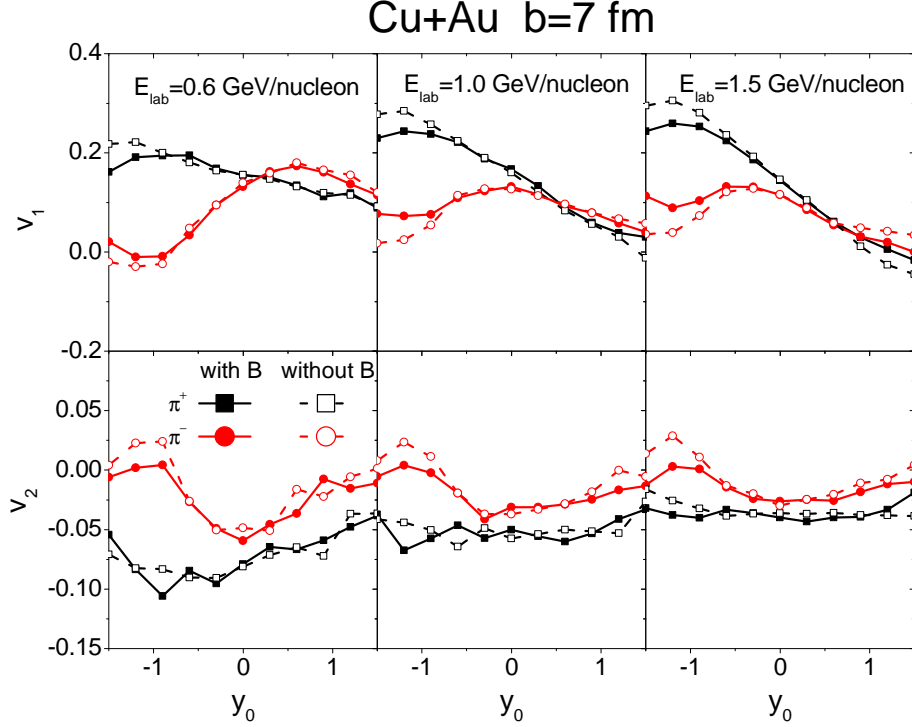
FIG. 16. (Color online) v_1 and v_2 of charged pions as a function of normalized center-of-mass rapidity in Cu+Au collisions at E_{lab}=0.6, 1, 1.5 GeV/nucleon with b=7 fm.

thus they are not strongly affected by the magnetic field.

Our results on π^-/π^+ raito and v_2^n-v_2^p suggest that the magnetic field effects could be comparable to the differences arising from different symmetry energy parameterizations. Effects of magnetic field should be included in future studies.

VI.   SUMMARY AND OUTLOOK

In summary, within the transport model UrQMD, the time evolution and space distribution of internal magnetic field are calculated. The magnetic field strength is found to reach about $eB = 470$ MeV^2 ($B = 8 \times 10^{16}$ G) for Au+Au collision at E_{lab}=1 GeV/nucleon with impact parameter of 7 fm. The magnetic field in Cu+Au collisions exhibits somewhat different space distribution from that in Au+Au collisions. It is also found that the magnetic field has an effect on pion directed flow, significant at forward and backward rapidities, dependent of impact parameter. Our UrQMD calculation of the magnetic field effects on pion directed flow is qualitatively consistent with IBUU, but quantitatively different. In
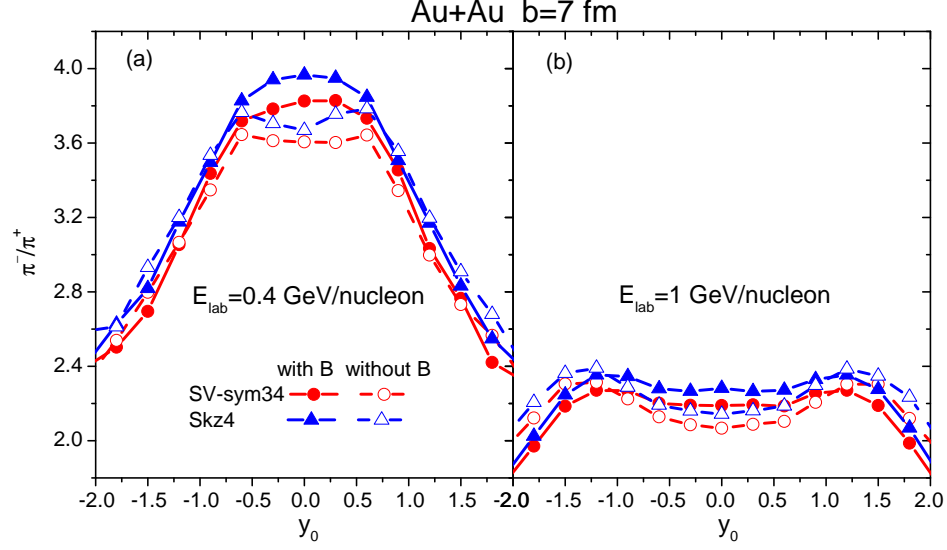
20

FIG. 17. (Color online) The π^-/π^+ yield ratio as a function of the normalized center-of-mass rapidity in Au+Au collisions at (a) E_{lab}=0.4 GeV/nucleon and (b) E_{lab}=1 GeV/nucleon with b=7 fm. Calculations with Skz4 (the corresponding slope parameter $L = 5.7$ MeV) and SV-sym34 ($L = 81$ MeV) interactions are shown.
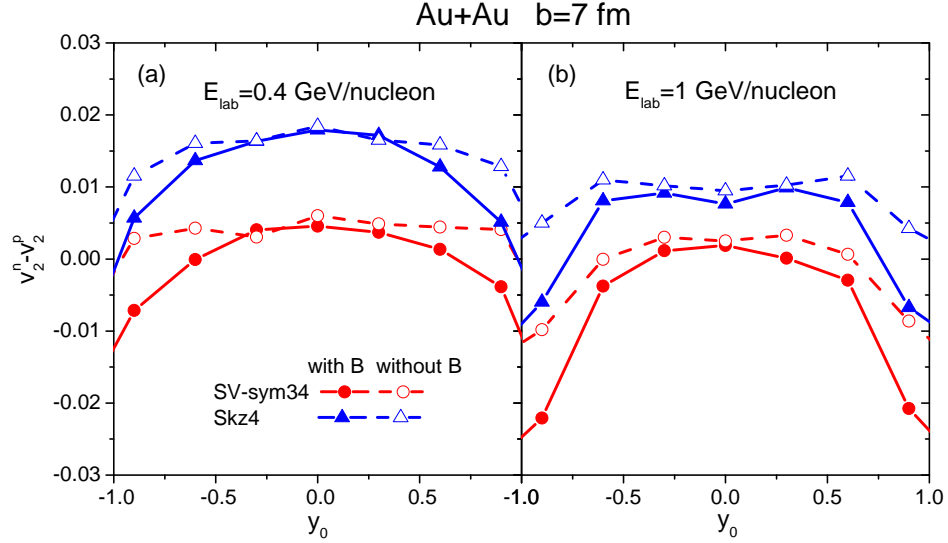

FIG. 18. (Color online) The elliptic flow difference between neutrons and protons v_2^n-v_2^p as a function of the normalized center-of-mass rapidity in Au+Au collisions at (a) E_{lab}=0.4 GeV/nucleon and (b) E_{lab}=1 GeV/nucleon with b=7 fm. Calculations with Skz4 ($L = 5.7$ MeV) and SV-sym34 ($L = 81$ MeV) interactions are shown.
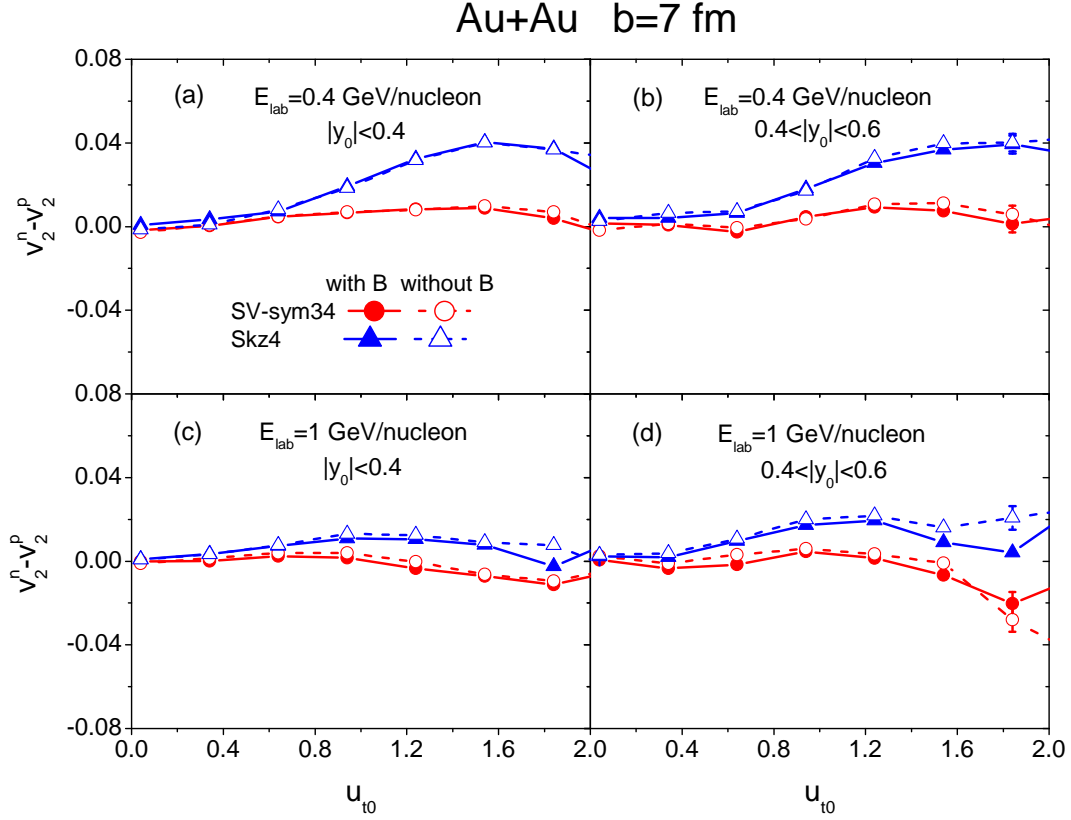
FIG. 19. (Color online) The elliptic flow difference between neutrons and protons v_2^n-v_2^p as a function of u_{t0} in Au+Au collisions at (a,b) E_{lab}=0.4 GeV/nucleon and (c,d) E_{lab}=1 GeV/nucleon with b=7 fm. Calculations with Skz4 ($L = 5.7$ MeV) and SV-sym34 ($L = 81$ MeV) interactions are shown.

addition, we found that the effects of the magnetic field on the π^-/π^+ ratio over the whole rapidity range and the elliptic flow difference v_2^n-v_2^p between neutrons and protons at forward and backward rapidities are on the same order as those from the nuclear symmetry energy. On the other hand, the v_2^n-v_2^p difference in the mid-rapidity region is not strongly affected by the magnetic field, and the total π^-/π^+ yield ratio is immune to it, indicating that they are still reliable probes to extract nuclear symmetry energy without considering magnetic field. In light of these results, it is advisable to include the magnetic field effects in future studies using pion flow, pion yield ratio and nucleon elliptic flow difference to probe the symmetry energy at super saturation densities.

ACKNOWLEDGMENTS

[1] J. P. Blaizot. Nuclear Compressibilities. *Phys. Rept.*, 64:171–248, 1980.

[2] Horst Stoecker and W. Greiner. High-Energy Heavy Ion Collisions: Probing the Equation of State of Highly Excited Hadronic Matter. *Phys. Rept.*, 137:277–392, 1986.

[3] V. Baran, M. Colonna, V. Greco, and M. Di Toro. Reaction dynamics with exotic beams. *Phys. Rept.*, 410:335–466, 2005.

[4] Bao-An Li, Lie-Wen Chen, and Che Ming Ko. Recent Progress and New Challenges in Isospin Physics with Heavy-Ion Reactions. *Phys. Rept.*, 464:113–281, 2008.

[5] Pawel Danielewicz, Roy Lacey, and William G. Lynch. Determination of the equation of state of dense matter. *Science*, 298:1592–1596, 2002.

[6] M. Dutra, O. Lourenco, J. S. Sa Martins, A. Delfino, J. R. Stone, and P. D. Stevenson. Skyrme Interaction and Nuclear Matter Constraints. *Phys. Rev.*, C85:035201, 2012.

[7] A. Le Fvre, Y. Leifels, W. Reisdorf, J. Aichelin, and Ch. Hartnack. Constraining the nuclear matter equation of state around twice saturation density. *Nucl. Phys.*, A945:112–133, 2016.

[8] Yongjia Wang, Chenchen Guo, Qingfeng Li, Arnaud Le Fvre, Yvonne Leifels, and Wolfgang Trautmann. Determination of the nuclear incompressibility from the rapidity-dependent elliptic flow in heavy-ion collisions at beam energies 0.4 A 1.0 A GeV. *Phys. Lett.*, B778:207–212, 2018.

[9] M. B. Tsang et al. Constraints on the symmetry energy and neutron skins from experiments and theory. *Phys. Rev.*, C86:015803, 2012.

[10] James M. Lattimer and Yeunhwan Lim. Constraining the Symmetry Parameters of the Nuclear Interaction. *Astrophys. J.*, 771:51, 2013.

[11] Bao-An Li, Angels Ramos, Giuseppe Verde, and Isaac Vidana. Topical issue on nuclear symmetry energy. *Eur. Phys. J.*, A50:9, 2014.

[12] P. Russotto et al. Results of the ASY-EOS experiment at GSI: The symmetry energy at suprasaturation density. *Phys. Rev.*, C94(3):034608, 2016.

[13] Andrew W. Steiner, Madappa Prakash, James M. Lattimer, and Paul J. Ellis. Isospin asymmetry in nuclei and neutron stars. *Phys. Rept.*, 411:325–375, 2005.

[14] James M. Lattimer and Maddapa Prakash. Neutron Star Observations: Prognosis for Equation of State Constraints. *Phys. Rept.*, 442:109–165, 2007.

[15] M. Di Toro, V. Baran, M. Colonna, and V. Greco. Probing the Nuclear Symmetry Energy with Heavy Ion Collisions. *J. Phys.*, G37:083101, 2010.

[16] LiMing L, Han Yi, ZhiGang Xiao, Ming Shao, Song Zhang, GuoQing Xiao, and Nu Xu. Conceptual design of the HIRFL-CSR external-target experiment. *Sci. China Phys. Mech. Astron.*, 60(1):012021, 2017.

[17] Zhigang Xiao, Bao-An Li, Lie-Wen Chen, Gao-Chan Yong, and Ming Zhang. Circumstantial Evidence for a Soft Nuclear Symmetry Energy at Suprasaturation Densities. *Phys. Rev. Lett.*, 102:062502, 2009.

[18] P. Russotto et al. Symmetry energy from elliptic flow in ^{197}Au $+^{197}$Au. *Phys. Lett.*, B697:471–476, 2011.

[19] M. D. Cozma, Y. Leifels, W. Trautmann, Q. Li, and P. Russotto. Toward a model-independent constraint of the high-density dependence of the symmetry energy. *Phys. Rev.*, C88(4):044912, 2013.

[20] X. Roca-Maza, M. Brenna, B. K. Agrawal, P. F. Bortignon, G. Col, Li-Gang Cao, N. Paar, and D. Vretenar. Giant Quadrupole Resonances in 208Pb, the nuclear symmetry energy and the neutron skin thickness. *Phys. Rev.*, C87(3):034301, 2013.

[21] Zhen Zhang and Lie-Wen Chen. Constraining the symmetry energy at subsaturation densities using isotope binding energy difference and neutron skin thickness. *Phys. Lett.*, B726:234–238, 2013.

[22] B. Alex Brown. Constraints on the Skyrme Equations of State from Properties of Doubly Magic Nuclei. *Phys. Rev. Lett.*, 111(23):232502, 2013.

[23] Pawel Danielewicz and Jenny Lee. Symmetry Energy II: Isobaric Analog States. *Nucl. Phys.*, A922:1–70, 2014.

[24] Ning Wang, Min Liu, Li Ou, and Yingxun Zhang. Properties of nuclear matter from macroscopicmicroscopic mass formulas. *Phys. Lett.*, B751:553–558, 2015.

[25] Johann Rafelski and Berndt Müller. Magnetic splitting of quasimolecular electronic states in strong fields. *Phys. Rev. Lett.*, 36:517–520, Mar 1976.

[26] Dmitri E. Kharzeev, Larry D. McLerran, and Harmen J. Warringa. The effects of topological charge change in heavy ion collisions: event by event p and cp violation. *Nuclear Physics A*, 803(3):227 – 253, 2008.

[27] Wei-Tian Deng and Xu-Guang Huang. Event-by-event generation of electromagnetic fields in heavy-ion collisions. *Phys. Rev. C*, 85:044907, 2012.

[28] Hao-Jie Xu, Xiaobao Wang, Hanlin Li, Jie Zhao, Zi-Wei Lin, Caiwan Shen, and Fuqiang Wang. Importance of isobar density distributions on the chiral magnetic effect search. *Phys. Rev. Lett.*, 121(2):022301, 2018.

[29] Li Ou and Bao-An Li. Magnetic effects in heavy-ion collisions at intermediate energies. *Phys. Rev. C*, 84:064605, 2011.

[30] Wen-Mei Guo, Gao-Chan Yong, Yongjia Wang, Qingfeng Li, Hongfei Zhang, and Wei Zuo. Model dependence of isospin sensitive observables at high densities. *Phys. Lett. B*, 726:211–217, 2013.

[31] Wen-Mei Guo, Gao-Chan Yong, Yongjia Wang, Qingfeng Li, Hongfei Zhang, and Wei Zuo. Normal or abnormal isospin-fractionation as a qualitative probe of nuclear symmetry energy at supradensities. *Phys. Lett.*, B738:397–400, 2014.

[32] V. Voronyuk, V. D. Toneev, S. A. Voloshin, and W. Cassing. Charge-dependent directed flow in asymmetric nuclear collisions. *Phys. Rev. C*, 90(6):064903, 2014.

[33] V. D. Toneev, V. Voronyuk, E. E. Kolomeitsev, and W. Cassing. Directed flow in asymmetric nucleus-nucleus collisions and the inverse Landau-Pomeranchuk-Migdal effect. *Phys. Rev. C*, 95(3):034911, 2017.

[34] S. A. Bass et al. Microscopic models for ultrarelativistic heavy ion collisions. *Prog. Part. Nucl. Phys.*, 41:255–369, 1998.

[35] M. Bleicher et al. Relativistic hadron hadron collisions in the ultrarelativistic quantum molecular dynamics model. *J. Phys. G*, 25:1859–1896, 1999.

[36] Qingfeng Li, Caiwan Shen, Chenchen Guo, Yongjia Wang, Zhuxia Li, J. Lukasik, and W. Trautmann. Nonequilibrium dynamics in heavy-ion collisions at low energies available

at the GSI Schwerionen Synchrotron. *Phys. Rev. C*, 83:044617, 2011.

[37] Qingfeng Li, G. Graf, and Marcus Bleicher. UrQMD calculations of two-pion HBT correlations in central Pb-Pb collisions at $\sqrt{s_{NN}} = 2.76$ TeV. *Phys. Rev. C*, 85:034908, 2012.

[38] Jorg Aichelin. quantum molecular dynamicsa dynamical microscopic n-body approach to investigate fragment formation and the nuclear equation of state in heavy ion collisions. *Physics Reports*, 202(5):233 – 360, 1991.

[39] Yongjia Wang, Chenchen Guo, Qingfeng Li, Hongfei Zhang, Y. Leifels, and W. Trautmann. Constraining the high-density nuclear symmetry energy with the transverse-momentum dependent elliptic flow. *Phys. Rev. C*, 89(4):044603, 2014.

[40] Yongjia Wang, Chenchen Guo, Qingfeng Li, Zhuxia Li, Jun Su, and Hongfei Zhang. Influence of differential elastic nucleon-nucleon cross section on stopping and collective flow in heavy-ion collisions at intermediate energies. *Phys. Rev.*, C94(2):024608, 2016.

[41] QingFeng Li, YongJia Wang, XiaoBao Wang, and CaiWan Shen. Rapidity distribution of protons from the potential version of UrQMD model and the traditional coalescence afterburner. *Sci. China Phys. Mech. Astron.*, 59(2):622001, 2016.

[42] LiYan Zou, Miao Li, ChenChen Guo, YongJia Wang, QingFeng Li, and Ling Liu. Influence of the time-step on the production of free nucleons and pions from heavy-ion collisions around 1 GeV/nucleon. *Sci. China Phys. Mech. Astron.*, 59(12):122011, 2016. [Erratum: Sci. China Phys. Mech. Astron.60,no.2,022051(2017)].

[43] Yangyang Liu, Yongjia Wang, Qingfeng Li, and Ling Liu. Collective flows of pions in Au+Au collisions at energies 1.0 and 1.5 GeV/nucleon. *Phys. Rev.*, C97(3):034602, 2018.

[44] YuShan Du, YongJia Wang, QingFeng Li, and Ling Liu. The effect of Lorentz-like force on collective flows of K$^+$ in Au+Au collisions at 1.5 GeV/nucleon. *Sci. China Phys. Mech. Astron.*, 61(6):062011, 2018.

[45] Pengcheng Li, Yongjia Wang, Qingfeng Li, Chenchen Guo, and Hongfei Zhang. Effects of the in-medium nucleon-nucleon cross section on collective flow and nuclear stopping in heavy-ion collisions in the Fermi-energy domain. *Phys. Rev.*, C97(4):044620, 2018.

[46] John David Jackson. Classical Electrodynamics Third Edition. 1998.

[47] V. Voronyuk, V. D. Toneev, W. Cassing, E. L. Bratkovskaya, V. P. Konchakovski, and S. A. Voloshin. Electromagnetic field evolution in relativistic heavy-ion collisions. *Phys. Rev. C*, 83:054911, 2011.

[48] W. Reisdorf et al. Systematics of central heavy ion collisions in the 1A GeV regime. *Nucl. Phys.*, A848:366–427, 2010.

[49] Bao-An Li. High density behavior of nuclear symmetry energy and high-energy heavy ion collisions. *Nucl. Phys.*, A708:365–390, 2002.

[50] M. D. Cozma. The impact of energy conservation in transport models on the π^-/π^+ multiplicity ratio in heavy-ion collisions and the symmetry energy. *Phys. Lett.*, B753:166–172, 2016.

[51] Bao-An Li. Symmetry potential of $\Delta(1232)$ resonance and its effects on the π^-/π^+ ratio in heavy-ion collisions near the pion-production threshold. *Phys. Rev.*, C92(3):034603, 2015.

[52] Zhen Zhang and Che Ming Ko. Medium effects on pion production in heavy ion collisions. *Phys. Rev.*, C95(6):064604, 2017.

[53] Zhen Zhang and Che Ming Ko. Effects of energy conservation on equilibrium properties of hot asymmetric nuclear matter. *Phys. Rev.*, C97(1):014610, 2018.

[54] Jun Xu. Transport approaches for the description of intermediate-energy heavy-ion collisions. *Prog. Part. Nucl. Phys.*, 106:312–359, 2019.

[55] Akira Ono et al. Comparison of heavy-ion transport simulations: Collision integral with pions and Δ resonances in a box. 2019.